International Journal of Mechanical, Industrial and Aerospace Sciences
ISSN: 2517-9950
Vol:12, No:3, 2018

Effect of Assumptions of Normal Shock Location on the Design of Supersonic Ejectors for Refrigeration

Payam Haghparast, Mikhail V. Sorin, Hakim Nesreddine

***Abstract*—**The complex oblique shock phenomenon can be simply assumed as a normal shock at the constant area section to simulate a sharp pressure increase and velocity decrease in 1-D thermodynamic models. The assumed normal shock location is one of the greatest sources of error in ejector thermodynamic models. Most researchers consider an arbitrary location without justifying it. Our study compares the effect of normal shock place on ejector dimensions in 1-D models. To this aim, two different ejector experimental test benches, a constant area-mixing ejector (CAM) and a constant pressure-mixing (CPM) are considered, with different known geometries, operating conditions and working fluids (R245fa, R141b). In the first step, in order to evaluate the real value of the efficiencies in the different ejector parts and critical back pressure, a CFD model was built and validated by experimental data for two types of ejectors. These reference data are then used as input to the 1D model to calculate the lengths and the diameters of the ejectors. Afterwards, the design output geometry calculated by the 1D model is compared directly with the corresponding experimental geometry. It was found that there is a good agreement between the ejector dimensions obtained by the 1D model, for both CAM and CPM, with experimental ejector data. Furthermore, it is shown that normal shock place affects only the constant area length as it is proven that the inlet normal shock assumption results in more accurate length. Taking into account previous 1D models, the results suggest the use of the assumed normal shock location at the inlet of the constant area duct to design the supersonic ejectors.

***Keywords*—**1D model, constant area-mixing, constant pressure-mixing, normal shock location, ejector dimensions.

NOMENCLATURE

A	Cross section area, mm^2
D	Diameter, mm
h	Specific enthalpy, $kJ.kg^{-1}$
L	Length, m
$\dot{m}$	Mass flow rate, $kg.s^{-1}$
M	Mach number
p	Pressure, kPa
PR	Pressure ratio (pressure lift)
s	Specific entropy, $kJ.kg^{-1} K^{-1}$
T	Temperature, K
u	Velocity, $m.s^{-1}$
v	Specific volume, $m^3.kg^{-1}$
X	Position of nozzle exit, mm

Greek symbols

η	Efficiency
φ	Half-angle, deg
ω	Entrainment ratio = $\dot{m}_s.\dot{m}_p^{-1}$ (-)
ρ	Density, $kg.m^{-3}$

Subscripts

d	Downstream of shock
diff	Diffuser
e	Exit
ejec	Ejector
is	Isentropic
mix	Mixing
out	Outlet
pol	Polytropic
pr	Primary nozzle
sec	Secondary nozzle
Th	Thermodynamic
th	Ejector throat
tot	Total
u	Upstream of shock

Acronyms

CAM	Constant area mixing
CPM	Constant pressure mixing
NI	Normal shock at the inlet of the constant area duct
NO	Normal shock at the outlet of the constant area duct

I. INTRODUCTION

AN ejector is an apparatus which creates vacuum by accelerating a gas, vapour or liquid in a nozzle. It can therefore be used to entrain a secondary or suction fluid. Ejectors are widely used in refrigeration systems. Ejector refrigeration systems usually have low maintenance cost because they operate without a compressor. Fig. 2 illustrates a typical ejector construction including ejector geometry, parts and main cross-sections. Convergent–divergent nozzle, suction chamber attached to a constant area duct and diffuser are the most important parts of an ejector. Many theoretical and experimental studies have been carried out to enhance the performance of ejectors in recent years. Among these studies, the effect of the lengths and diameters on the ejector performance and the selection of an appropriate refrigerant proportional to the ejector application are considerably investigated.

Some researchers have investigated the effect of ejector geometry on its performance, such as nozzle exit location, mixing chamber/nozzle area ratio, and nozzle design. Cizungu et al. [1] optimized the ejector geometry to achieve maximum values for either the entrainment ratio or the pressure ratio. Vereda et al. [2] and Elbel and Hrnjak [3] experimentally

Payam Haghparast is with the Mechanical Engineering Department, Université de Sherbrooke, Sherbrooke, QC, J1K 2R1, Canada

Mikhail V. Sorin is with the Mechanical Engineering Department, Université de Sherbrooke, Sherbrooke, QC, J1K 2R1, Canada, e-mail: Mikhail.V.Sorin@USherbrooke.ca, phone: +1 (819) 821 8000 x 62155).

Hakim Nesreddine is with the Hydro-Québec, 600 Rue de la montagne, Shawinigan, QC, G9N 7N5, Canada.

studied different ejector dimensions, such as the sizing of the motive nozzle and the diffuser.

Banasiak et al. [4] examined different ejector configurations in order to achieve optimum ejector geometry. They used various lengths and diameters of the mixing duct and various angles of divergence for the diffuser. Nakagawa et al. [5] experimentally analyzed the effect of the mixing length on ejector system performance. Chen et al. [6] and Gil and Kasperski [7] studied the effect of different refrigerants on the ejector efficiency in the refrigeration systems. A review of recent developments in advanced ejector technology can be found in [8].

Researchers always make assumptions for theoretical analyses of the ejectors. one of the most important assumptions in 1-D thermodynamic models is to consider a normal shock in constant area duct to justify the complex oblique shock phenomenon. The Mach number of the working fluid is larger than 1 before this shock, whereas smaller than 1 after the shock. This process is irreversible and cannot be treated as isentropic [9].

Referring to the assumptions proposed by different researchers, three different places of the constant area duct have been usually considered. Some researchers consider a normal shock at the end of the constant area section for thermodynamic modeling, without justification [10]-[12]. Some researchers assume a place at the inlet of the constant area section [13]. Some consider a place inside the constant area section [9]. Therefore, determination of the appropriate place of the normal shock can help in achieving a more accurate simulation.

The objective of the present study is to develop a more accurate 1D model to design the supersonic ejectors. The effects of the normal shock assumption on the ejector dimensions and mixing efficiency are evaluated. All ejector geometries are calculated by a developed thermodynamic model. This model is applicable for both types of the ejectors, CPM and CAM. The obtained dimensions by 1D model based on different normal shock location are compared to experimental data in order to determine more accurate assumption.

II. Ejector Analysis Procedure

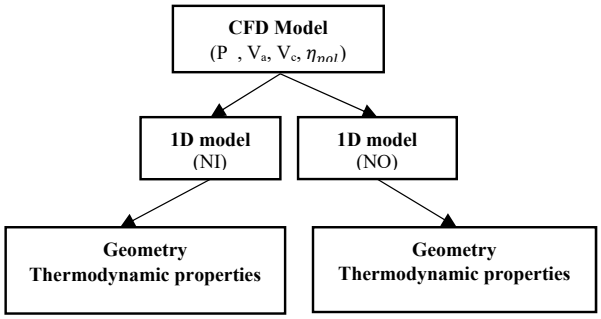

Fig. 1 Procedure for the optimization of calculating ejector parameters based on normal shock assumptions

Fig. 1 shows the analysis procedure used in the present research to determine the more accurate assumption of the normal shock location. Depending on where the normal shock takes place, at inlet or outlet of the constant area duct, the geometries and properties are calculated and compared with experimental data. To determine dimensions by 1D models, it is first necessary to extract some important data from CFD and experimental models. The critical back pressure, efficiencies and boundary conditions are the most important data obtained from corresponding models.

III. Ejector Operation and Geometry

Fig. 2 illustrates the geometry, parts and main cross-sections of ejectors under investigation. Two different types of the ejector test benches according to the position of the nozzle exit are considered, constant-area mixing (CAM) and constant-pressure mixing (CPM). For case 1 (CAM), available experimental ejector data were used from the Hydro-Québec laboratory in Shawinigan. For case 2 (CAM), the experimental data of Huang et al. [14] were used.

As shown in Fig. 2, the ejector design can be classified into two categories according to the position of the nozzle. For the nozzle with its exit located within the constant-area section of an ejector, the mixing of the primary and the entrained flows occurs inside the constant-area section and the ejector is known as “constant-area mixing ejector”. For the nozzle with its exit located within the suction chamber which is in front of the constant-area section, the ejector is referred as “constant-pressure mixing ejector”. For this kind of ejector, it was assumed that the mixing of the primary and the entrained streams occurs in the suction chamber with a uniform or constant pressure [14] . It is known that the constant-pressure ejector has a better performance than the constant-area ejector and is thus widely used [15], [16].

TABLE I
Operating Condition

Parameter	Case# 1 (CAM)	Case# 2 (CPM)
Working fluid	R245fa, **Real Fluid**	R141b, **Real Fluid**
P4, T4 (Primary Inlet)	480.6 kPa, 352.45 K	604 kPa, 368.15 K
P6, T6 (Secondary Inlet)	100.1 kPa, 303.75 K	40 kPa, 283.45 K

TABLE II
Geometry of the Ejectors (Case# 1 & 2)

D [mm]	Case# 1	Case# 2	L, X [mm]	Case# 1	Case# 2	φ [deg]	Case# 1	Case# 2
Da	32.08	8.251	L_1	100.9	15.4	φ_1	5	10
D_{th}	14.42	2.810	L_2	46	35.4	φ_2	5	3
D_{7p}	22.47	6.518	X	7.08	4.2	φ_3	6.99	5
D_7	28.47	9.527	L_4	223.77	146.0	φ_4	5.98	4
D_8= D_u=D_d	28.47	8.794	L_5	46	121.6	φ_5	22.96	
Dc	38.10	25.803	L_{tot}	416.67	322.6			

Operating conditions, as well as the geometry of the ejectors, are illustrated in Tables I and II. Further, a flowchart of the main inputs and outputs of the models is introduced in Fig. 3.

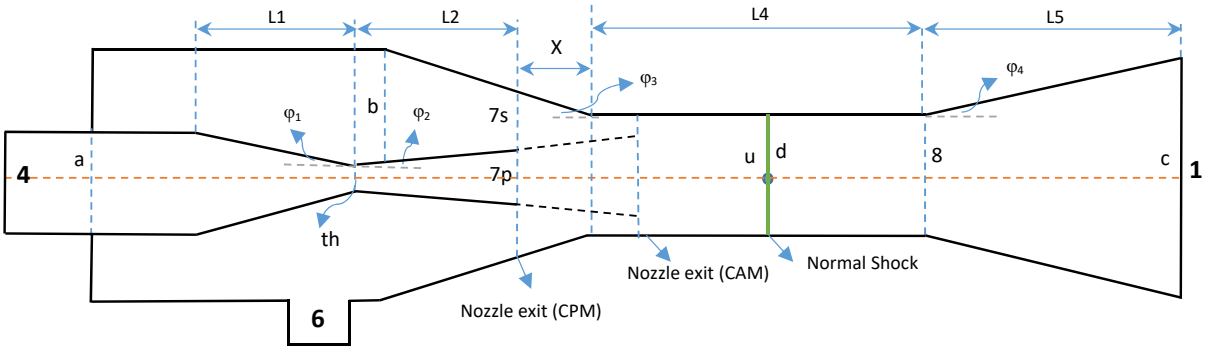

Fig. 2 Ejector geometry, parts and main cross-sections

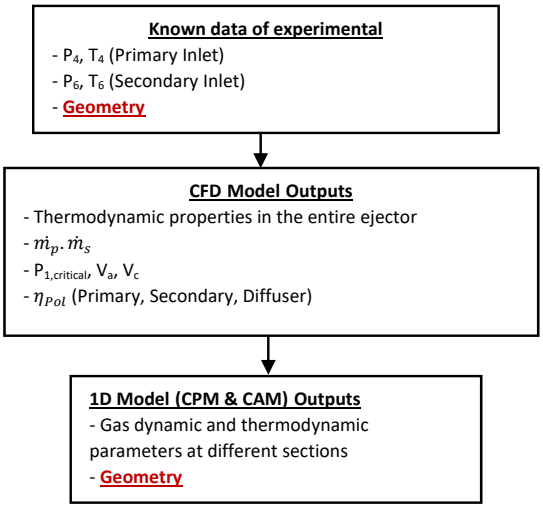

Fig. 3 Overall procedure for calculating the inputs and outputs

IV. CFD Model

Numerical simulations have been carried out to determine some important values such as critical back pressure (point c) and polytropic efficiencies, velocity value at section a and c (V_a and V_c) for two test benches. The numerical values of the calculated dimensions by 1D models are extremely dependent on these CFD reference values.

A. CFD Setting

A numerical investigation has been carried out by means of ANSYS Workbench V17 for mesh generation and ANSYS Fluent V17 to solve the governing equations by control volume method. Based on successful implementations reported in the literature [17], turbulence effects in the ejector have been modeled using the k-ω SST turbulence model. Second order accurate discretization scheme coupled with a density-based implicit solver is used. The energy equation is solved in a second step and density is computed through the REFPROP v 9.1 database equation [18]. The conservation equations governing the fluid flow in the ejector are of the compressible, steady state, axisymmetric form and all the walls are assumed adiabatic. In conclusion, the main features of the numerical scheme can be summarized in Table III.

TABLE III
CFD Settings (Case# 1 & 2)

Working fluid	R245fa, Real fluid (Case# 1) R141b, Real fluid (Case# 2)
Turbulence Model	k-w SST(HRN)
Solver	Pressure based
Numerical schemes	Coupled, Pressure: PRESTO! Momentum, Turbulence, Energy: 2nd order Upwind
Convergence criteria	Residuals RMS<1×10-5 Mass imbalances<1%

B. Details of the Mesh Grid Used in the CFD Calculations

Before proceeding the main calculation, a grid convergence study was performed to ensure overall mesh-independent results. Finally, 5.66×105 quadrilateral cells for Case# 1 and 6.81×105 quadrilateral cells for Case# 2 was considered sufficient to give satisfactory results in terms of entrainment ratio (Figs. 4 and 5). This mesh is refined from the primary nozzle lips along the shear layer and also close to walls in order to achieve an average value for the wall coordinate (y+), adequate for the application of a High-Reynolds approach [19].

C. Mach Contours of Various Back Pressures

After accelerating the secondary stream to sonic velocity and mixes with the primary stream in the constant area duct, the region of supersonic flow is terminated by a normal shock wave further down the duct or in the diffuser. Across the shock, pressure increases but Mach number (velocity) reduces to a subsonic value. The mixture of primary and secondary flows then passes through the subsonic diffuser where it converts kinetic energy into pressure energy by a recompression process to reach the back-pressure (condenser pressure) at near zero velocity. Fig. 6 shows Mach number contour plots of the different flow fields along the ejector and into the constant area duct.

According to the performance curves of the ejectors, the critical back pressure for case 1 is equal to 190.19 kPa and for case 2 is equal to 105.5 kPa. Table IV presents the calculated efficiencies for critical back pressures at fixed inlet conditions for two cases by CFD models.

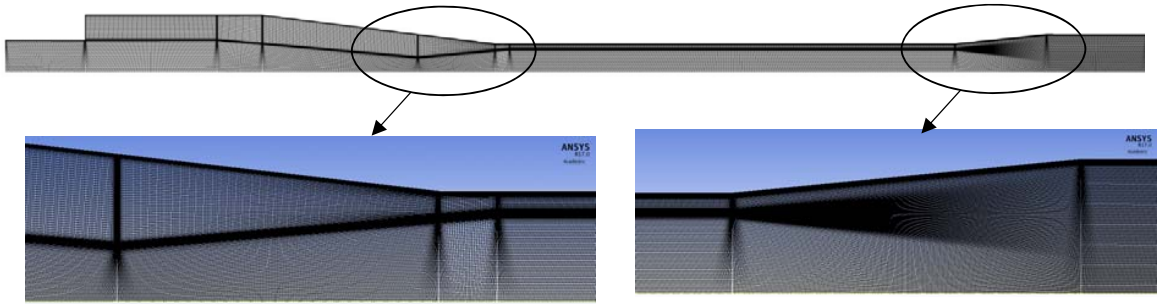

Fig. 4 Details of the mesh grid used in the CFD calculations for Case# 1 (CAM)

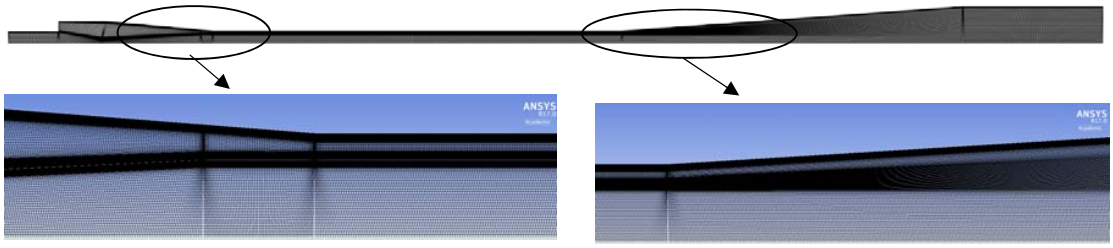

Fig. 5 Details of the mesh grid used in the CFD calculations for Case# 2 (CPM)

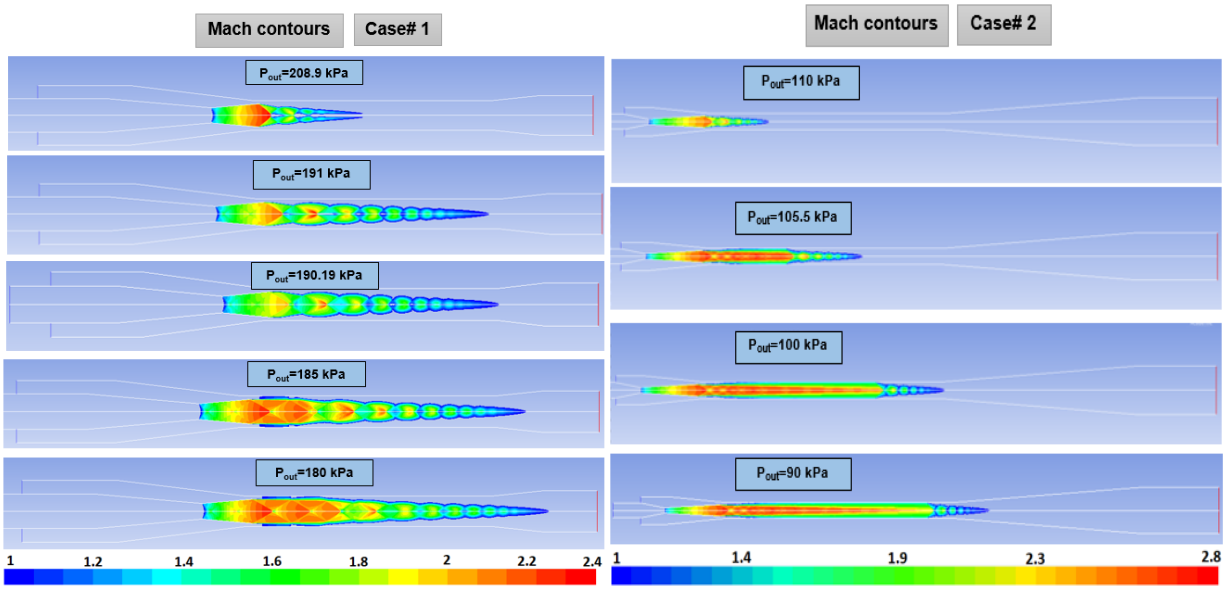

Fig. 6 Mach number plots of the ejectors at various back pressures for case# 1 and case# 2

TABLE IV
EFFICIENCIES ACCORDING TO THE CFD MODELS FOR CRITICAL BACK PRESSURE POINT FOR CASE 1 AND 2

	P_{out} (kPa)	PR	Polytropic (CFD)			Mixing (CFD)
	P1	P1/P6	Primary	Secondary	Diffuser	Mixing
Case 1	190.19	1.9	0.9757	0.9752	0.8211	0.9681
Case 2	105.5	2.644	0.9373	0.9352	0.9436	0.9137

V. THERMODYNAMIC MODEL

Among the different models, the model proposed by Galanis and Sorin [20] is able to calculate all ejector dimensions and fluid properties. In this study, a new model is developed which has the ability to simulate both types of ejectors, CPM and CAM for two assumed normal shock locations. A thermodynamic model is programmed in EES (Engineering Equation Solver) which includes relations for the fluid properties [21]. To simplify the analysis, some assumptions are considered [13]. Flow is one dimensional, compressible and steady state throughout the ejector. The primary and secondary fluids are identical vapors, with real fluid properties. Pressure, temperature, and mass flow are known from experimental data for both the primary and

secondary inlets. All fluid properties are uniform across their respective cross-sectional areas. Both primary and secondary fluids are choked (critical operation). The details of the calculation procedure for the CPM type of ejector by using the conception of polytropic efficiency are described in the following steps. In each step, inputs, outputs and appropriate equations are introduced.

The calculation begins with the expansion and subsonic acceleration of the secondary fluid from the given stagnation conditions P_6 and T_6, taking into consideration the known flow rate $\dot{m}_s$. Finally, it finishes with deceleration of mixing stream at diffuser. The governing equations account for the conservation of the mass, momentum, and energy are presented below.

- **Cross-section 7s:** To calculate conditions at Cross-section (7s), energy and mass conservation are solved by progressively decreasing the pressure (P) to maximize ($\dot{m}_s$/A). This procedure is repeated until the ratio ($\dot{m}_s$/A) reaches a maximum value. Since the flowrate $\dot{m}_s$ is known it is then possible to calculate the area A_{7s}. (Critical operation)

$$P_j = P_{j-1} - \Delta P_s \quad (1)$$

$$\eta_{pol,s} = (h_{j-1} - h_j)/(h_{j-1} - h_{j,is}) \quad (2)$$

$$h_{j.is} = h(P_j, s_{j-1}) \quad (3)$$

$$h_6 = h_j + 0.5V_j^2 \quad (4)$$

$$\dot{m}_s/A_j = V_j/\nu_j \quad (5)$$

$$\nu_j = \nu(P_j, h_j) \quad \text{and} \quad s_j = s(P_j, h_j) \quad (6)$$

- **Cross-section b:** By using V_b obtained from CFD, it is possible to determine the gas dynamic and thermodynamic parameters at cross-section (b) as well as the area A_b.
- **Cross-section throat:** The primary flow is always choked. The same procedure is applied to the expansion of the primary stream in the converging-diverging nozzle and generates the conditions at its throat (th). Since the flowrate $\dot{m}_p$ is fixed, the area A_{th} and its diameter D_{th} are both calculated.
- **Cross-section 7p:** Since $P_{7p} = P_{7s}$, it is possible to continue the procedure in order to determine the conditions of the primary stream at state (7p) and to calculate the area A_{7p} from mass conservation as well as the corresponding diameter D_{7p}. From $A_7 = A_{7p} + A_{7s}$ it is then possible to calculate the diameter D_7. The isentropic efficiency of the primary stream expansion from (4) to (7p) can then also be determined.
- **Cross-section a:** To calculate the gas dynamic and thermodynamic parameters at Cross-section (a) as well as the area (A_a), the V_a obtained from CFD is used.
- **Cross-section u (**before normal shock**):** By applying the equations expressing mass, energy and momentum conservation for the control volume between cross-sections (7) and (u), immediately upstream of the shock.

$$\dot{m}_p + \dot{m}_s = V_u A_u/\upsilon_u \quad (7)$$

$$h_4 + \omega h_6 = (1+\omega)(h_u + 0.5V_u^2) \quad (8)$$

$$(P_{7p}A_{7p} + \dot{m}_p V_{7p}) + (P_{7s}A_{7s} + \dot{m}_s V_{7s}) - F_f = P_u A_u + (\dot{m}_p + \dot{m}_s)V_u \quad (9)$$

By simplifying (9), we have:

$$V_{7p} + \omega V_{7s} = (1+\omega)V_u \quad (10)$$

- **Cross-section d (**after normal shock**):** Since $A_u = A_d$, with the expressions of mass, energy and momentum conservation.

$$\dot{m}_p + \dot{m}_s = V_d A_d/\upsilon_d \quad (11)$$

$$h_4 + \omega h_6 = (1+\omega)(h_d + 0.5V_d^2) \quad (12)$$

$$(P_d + P_u) = (\dot{m}_p + \dot{m}_s)(V_u - V_d) \quad (13)$$

- **Cross-section 8 (**inlet of the diffuser**):** By using the known back pressure value and expressing mass, energy and momentum conservation for the control volume between cross-sections (8) and (1), the ejector outlet, we have (14)-(19). This procedure is repeated until A_j becomes equal to $A_d = A_u$. The corresponding enthalpy, pressure, entropy, and velocity are those of the mixture at cross-section (8). Mixing efficiency also can be calculated using (20).

$$h_j = h_{j-1} - \Delta h \quad (14)$$

$$h_{(j-1),is} = h_j + (\Delta h \eta_{pol,D}) \quad (15)$$

$$s_j = s_{(j-1),is} = s(p_{j-1}, h_{(j-1),is}) \quad (16)$$

$$P_j = P(h_j, s_j) \; and \; \nu_j = \nu(P_j, h_j) \quad (17)$$

$$h_4 + \omega h_6 = (1+\omega)(h_j + 0.5V_j^2) \quad (18)$$

$$A_j = (\dot{m}_p + \dot{m}_s)\left(\frac{\nu_j}{V_j}\right) \quad (19)$$

$$\eta_{mix} = 1 - \frac{F_f}{\dot{m}_p V_{7p} + \dot{m}_s V_{7s}} \quad (20)$$

$$F_f = (P_{7p}A_{7p} + \dot{m}_p V_{7p}) + (P_{7s}A_{7s} + \dot{m}_s V_{7s}) - P_8 A_8 - (\dot{m}_p + \dot{m}_s)V_8 \quad (21)$$

- **Cross-section c (**before outlet**):** By using V_c obtained from CFD, it is possible to determine the thermodynamic properties at Cross-section (c) as well as the area A_c.

$$L_1 = (D_a - D_{th})/2tan(\varphi_1) \quad (22)$$

$$L_2 = (D_{7p} - D_{th})/2tan(\varphi_2) \quad (23)$$

$$L_5 = (D_c - D_8)/2tan(\varphi_4) \quad (24)$$

$$P_d A_d + (\dot{m}_p + \dot{m}_s)V_d - F_f = P_8 A_8 + (\dot{m}_p + \dot{m}_s)V_8 \quad \text{(NI)}$$
$$P_u A_u + (\dot{m}_p + \dot{m}_s)V_u + F_f = P_7 A_7 + (\dot{m}_p + \dot{m}_s)V_7 \quad \text{(NO)} \quad (25)$$

$$\Delta P = F_f/A_8 = f\,(L_4/D_8)(\rho V^2/2) \text{ (Darcy equation)}$$
$$L_4 = F_f/(f\,(A_8/D_8)(\rho V^2/2)) \quad (26)$$

$$f = \left(\frac{1}{-2log\left(\frac{e}{3.7\,D} + \frac{2.51}{Re\sqrt{f}}\right)}\right)^2 \text{ (Colebrook equation)} \quad (27)$$

Absolute wall roughness for commercial new steel (e=0.046 mm) (Re>4000).

Calculation of nozzle exit position is as follows:

$$X = (D_7 - D_u)/2tan(\varphi_5) \text{ (CPM)} \quad (28)$$

$$X = (D_{7s})/2tan(\varphi_3) \text{ (CAM)} \quad (29)$$

VI. Results and Discussion

The effect of assuming that the normal shock location is within the constant area duct can be evaluated with the help of Tables V-VIII. The conclusion that can be drawn from these results is that the choice of the location of the normal shock only affects the constant area length (L_4) and the flow properties at sections u and d.

The absolute deviation of the L_4 from experimental dimension based on normal shock at the inlet is 3.9% for case 1 while it is 34.94% for normal shock at the outlet (Tables V and VI). Similarly, 6.24% and 66.84% deviations for case 2 are observed compared to experimental length for inlet and outlet normal shock assumption respectively (Tables VII and VIII).

TABLE V
Effect of the Assumed Normal Shock Location on Ejector Dimensions for Case 1 (CAM) ($P_{out, critical}$=190.19 kPa)

D, L, X [mm]	Experimental test bench	Normal Shock (inlet)	Error (%)	Normal Shock (outlet)	Error (%)
D_{th}	14.42	14.3	-0.8321	14.3	-0.8321
D_{7p}	22.47	21.57	-4.0053	21.57	-4.0053
D_7	28.47	27.71	-2.6694	27.71	-2.6694
D_8= D_u=D_d	28.47	27.71	-2.6694	27.71	-2.6694
D_c	38.10	38.16	0.1574	38.16	0.1574
L_1	100.9	99.77	-1.12	99.77	-1.12
L_2	46	41.53	-9.7173	41.53	-9.7173
L_4	223.77	232.5	3.9	145.6	34.94
L_5	46	49.9	8.4783	49.9	8.4783
L_{tot}	416.67	423.7	1.69	336.8	19.17

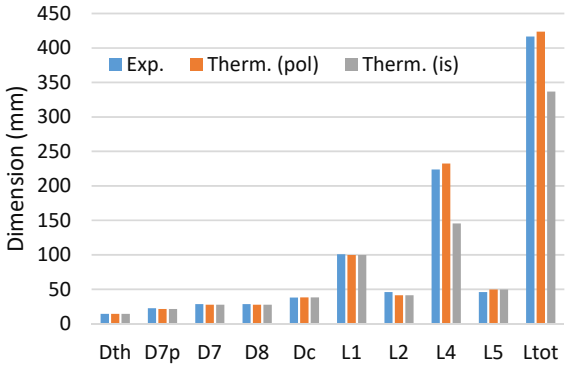

Fig. 7 Comparisons of dimensions for case 1 (CAM)

TABLE VI
Effect of the Assumed Normal Shock Location on Flow Properties at Sections u and d for Case 1 (CAM) ($P_{out, critical}$=190.19 kPa)

	States	P [kPa]	T [K]	V [m/s]	M [-]
1D model (NI)	u	54.63	301.37	243.9	1.748
1D model (NI)	d	170.9	332.88	84.15	0.5863
1D model (NO)	u	58.49	305.06	230.5	1.642
1D model (NO)	d	161.4	332.2	89.15	0.6205

TABLE VII
Effect of the Assumed Normal Shock Location on Ejector Dimensions for Case 2 (CPM) ($P_{out, critical}$=105.05 kPa)

D, L, X [mm]	Experimental test bench	Normal Shock (inlet)	Error (%)	Normal Shock (outlet)	Error (%)
D_{th}	2.810	2.834	0.8541	2.834	0.8541
D_{7p}	6.518	6.577	0.9052	6.577	0.9052
D_7	9.527	9.166	-3.789	9.166	-3.789
D_8	8.794	8.517	-3.15	8.517	-3.15
D_c	25.803	25.76	-0.167	25.76	-0.167
L_1	15.4	14.73	-4.351	14.73	-4.351
L_2	35.4	35.71	0.8757	35.71	0.8757
L_4	146	155.1	6.24	48.42	66.84
L_5	121.6	123.3	1.398	123.3	1.398
L_{tot}	322.6	328.8	1.92	225.9	29.97

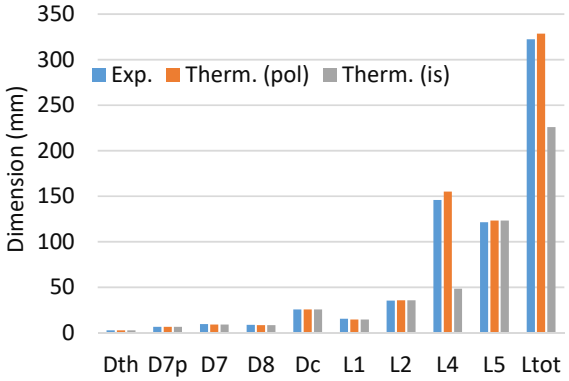

Fig. 8 Comparisons of dimensions for case 2 (CPM)

TABLE VIII
EFFECT OF THE ASSUMED NORMAL SHOCK LOCATION ON FLOW PROPERTIES AT SECTIONS U AND D FOR CASE 2 (CPM) ($P_{OUT, CRITICAL}$=105.05 KPA)

	States	P [kPa]	T [K]	V [m/s]	M [-]
1D model (NI)	u	23.36	281.9	302	2.044
1D model (NI)	d	101.7	338.43	81.97	0.5162
1D model (NO)	u	28.19	296.79	263.2	1.739
1D model (NO)	d	88.32	336.81	94.18	0.5928

VII. CONCLUSION

In the present study, the effect of the normal shock location on the design of a one-phase supersonic ejector was investigated. CFD technique first was used to evaluate the exact value of the efficiencies, critical back pressure and also more detailed information about the flow, density and temperature distributions in the ejector. Afterwards, data obtained from the CFD simulations were applied in the 1D thermodynamic models to calculate all ejector dimensions. To this aim, two test benches, a constant area-mixing ejector (CAM) and a CPM were considered with different geometries, working fluids and operating conditions.

It is shown that the present thermodynamic model is able to calculate precisely all ejector dimensions for both types of the ejectors compared to experimental dimensions over the entire range of operation. It is further found that the effect of normal shock place is only on constant area length (L_4) and flow properties at sections u and d. The value of the L_4 based on normal shock at the inlet is more accurate than normal shock at the outlet against experimental one. In conclusion, the research findings will be meaningful for researchers to have a better understanding of the normal shock assumption. The results show that when the normal shock assumed at the inlet of constant area duct, obtained dimensions by the 1D model are more accurate for both types of ejectors (CPM and CAM) compared to experimental dimensions.

ACKNOWLEDGMENT

The authors wish to thank Hydro-Québec laboratory Shawinigan for their valuable contribution during the ejector design used in the present paper. This project is a part of the Collaborative Research and Development (CRD) Grants Program at 'Université de Sherbrooke'. The authors also acknowledge the support of the Natural Sciences and Engineering Research Council of Canada, Rio Tinto Alcan and CanmetENERGY Research Center of Natural Resources Canada.

REFERENCES

[1] K. Cizungu, M. Groll, and Z. G. Ling, "Modelling and optimization of two-phase ejectors for cooling systems," *Appl. Therm. Eng.*, vol. 25, no. 13, pp. 1979–1994, 2005.

[2] C. Vereda, R. Ventas, A. Lecuona, and M. Venegas, "Study of an ejector-absorption refrigeration cycle with an adaptable ejector nozzle for different working conditions," *Appl. Energy*, vol. 97, pp. 305–312, 2012.

[3] S. Elbel and P. Hrnjak, "Experimental validation of a prototype ejector designed to reduce throttling losses encountered in transcritical R744 system operation," *Int. J. Refrig.*, vol. 31, no. 3, pp. 411–422, 2008.

[4] K. Banasiak, A. Hafner, and T. Andresen, "Experimental and numerical investigation of the influence of the two-phase ejector geometry on the performance of the R744 heat pump," *Int. J. Refrig.*, vol. 35, no. 6, pp. 1617–1625, 2012.

[5] M. Nakagawa, A. R. Marasigan, T. Matsukawa, and A. Kurashina, "Experimental investigation on the effect of mixing length on the performance of two-phase ejector for CO 2 refrigeration cycle with and without heat exchanger," *Int. J. Refrig.*, vol. 34, no. 7, pp. 1604–1613, 2011.

[6] J. Chen, H. Havtun, and B. Palm, "Parametric analysis of ejector working characteristics in the refrigeration system," *Appl. Therm. Eng.*, vol. 69, no. 1, pp. 130–142, 2014.

[7] B. Gil and J. Kasperski, "Efficiency analysis of alternative refrigerants for ejector cooling cycles," *Energy Convers. Manag.*, vol. 94, pp. 12–18, 2015.

[8] S. Elbel and N. Lawrence, "Review of recent developments in advanced ejector technology," *Int. J. Refrig.*, vol. 62, pp. 1–18, 2016.

[9] J. Bao, Y. Lin, and G. He, "Working fluids comparison and thermodynamic analysis of a transcritical power and ejector refrigeration cycle (TPERC)," *Int. J. Refrig.*, 2017.

[10] J. Lee, C. Lee, S. Baek, and S. Jeong, "Investigation of ejector-equipped Joule–Thomson refrigerator operating below 77 K," *Int. J. Refrig.*, vol. 78, pp. 93–107, 2017.

[11] Z. Ma, H. Bao, and A. P. Roskilly, "Thermodynamic modelling and parameter determination of ejector for ejection refrigeration systems," *Int. J. Refrig.*, vol. 75, pp. 117–128, 2017.

[12] G. Besagni, R. Mereu, F. Inzoli, and P. Chiesa, "Application of an integrated lumped parameter-CFD approach to evaluate the ejector-driven anode recirculation in a PEM fuel cell system," *Appl. Therm. Eng.*, vol. 121, pp. 628–651, 2017.

[13] M. Khennich, N. Galanis, and M. Sorin, "Effects of design conditions and irreversibilities on the dimensions of ejectors in refrigeration systems," *Appl. Energy*, vol. 179, pp. 1020–1031, 2016.

[14] B. J. Huang, J. M. Chang, C. P. Wang, and V. A. Petrenko, "A 1-D analysis of ejector performance," *Int. J. Refrig.*, vol. 22, no. 5, pp. 354–364, 1999.

[15] Keenan, E.P. Neumann, and F. Lustwerk J.H., "An investigation of ejector design by analysis and experiment," vol. J Appl Mech Trans ASME, 72 (1950), pp. 299–309, 1950.

[16] W. Chen, C. Shi, S. Zhang, H. Chen, D. Chong, and J. Yan, "Theoretical analysis of ejector refrigeration system performance under overall modes," *Appl. Energy*, 2016.

[17] S. Croquer, S. Poncet, and Z. Aidoun, "Turbulence modeling of a single-phase R134a supersonic ejector. Part 2: Local flow structure and exergy analysis," *Int. J. Refrig.*, vol. 61, pp. 153–165, 2016.

[18] NIST-REFPROP, v9.1., "NIST (2013). NIST Reference Fluid Thermodynamic and Transport Properties -REFPROP, v9.1." 2013.

[19] "ANSYS FLUENT 17.0." ANSYS FLUENT Theory Guide release 17.0, ANSYS Inc., 2017.

[20] N. Galanis and M. Sorin, "Ejector design and performance prediction," *Int. J. Therm. Sci.*, vol. 104, pp. 315–329, 2016.

[21] Klein, S., "Engineering Equation Solver.(EES)." Engineering Equation Solver. F-Chart Software., 2011.